



Electrochemical Formation of Si Films by Co-deposition of Si and Zn in Molten $\text{KF-KCl-K}_2\text{SiF}_6\text{-ZnCl}_2$ Systems



Wataru MOTEKI,[§] Yutaro NORIKAWA,^{§§} and Toshiyuki NOHIRA^{*,§§§}

Institute of Advanced Energy, Kyoto University, Gokasho, Uji, Kyoto 611-0011, Japan

* Corresponding author: nohira.toshiyuki.8r@kyoto-u.ac.jp, Tel.: + 81-774-38-3500, Fax: + 81-774-38-3499

ABSTRACT

Crystalline silicon solar cells have become the leading technology in solar cell manufacturing. However, conventional solar cell manufacturing methods are energy-intensive and inefficient. We previously developed an electrodeposition method that improved crystalline Si film production but faced limitations in grain size, which is crucial for minimizing recombination losses in polycrystalline Si solar cells. In this study, the co-deposition of Si and Zn on a graphite substrate is investigated to obtain large grain-sized Si films. Electrochemical measurements and electrolysis are conducted at 923 K in molten $\text{KF-KCl-K}_2\text{SiF}_6\text{-ZnCl}_2$ systems. Reduction currents corresponding to the reduction of Zn(II) and Si(IV) ions are observed at approximately $-2.6\text{ V vs. Cl}_2/\text{Cl}^-$ and -3.1 V , respectively in the cyclic voltammogram on a glassy carbon electrode. The optimal conditions for obtaining highly crystalline Si films are investigated by varying the ZnCl_2 concentration and current density. During co-deposition, a Si-Zn liquid alloy is deposited. Post-electrodeposition cross-sectional images reveal a Si layer on the graphite substrate with a Zn layer on top. After Zn removal, the Si films exhibit larger crystal sizes than those obtained without ZnCl_2 , indicating deposition through liquid alloying with Zn.

© The Author(s) 2024. Published by ECSJ. This is an open access article distributed under the terms of the Creative Commons Attribution-NonCommercial-ShareAlike 4.0 License (CC BY-NC-SA, <https://creativecommons.org/licenses/by-nc-sa/4.0/>), which permits non-commercial reuse, distribution, and reproduction in any medium by share-alike, provided the original work is properly cited. For permission for commercial reuse, please email to the corresponding author. [DOI: [10.5796/electrochemistry.24-00104](https://doi.org/10.5796/electrochemistry.24-00104)].



Keywords : Silicon, Liquid Metal, Molten Salt, Co-deposition

1. Introduction

In recent years, crystalline Si solar cells have dominated solar cell manufacturing, accounting for approximately 97% of total production.¹ Since the early 2000s, their production has been increasing every year, and their demand is expected to grow in the future. However, conventional manufacturing methods for solar cells are multi-step processes, including the Siemens method. This method has limitations due to high energy costs and low-yield processes.²

To address these issues, we had earlier developed a direct crystalline Si film formation method by electrodeposition.³⁻⁸ Using this method, researchers successfully electrodeposited crystalline Si from various high-temperature molten salts.³⁻³³ Among the high-temperature molten salts studied, we found KF-KCl molten salts have promising potential owing to their high fluoride content, which promotes dense and smooth crystalline Si films.^{2,3} KF and KCl are highly water-soluble and can thus be easily removed by rinsing.^{34,35} In addition, this method supports closed-cycle operation through chlorine generation at the counter electrode. In our previous study, we obtained Si films with a purity of 4N in this molten salt and confirmed the formation of Si films with p- and n-type semiconductor properties.⁷

However, one of the limitations of this method has been the small grain size of Si films. We confirmed that the grain size of Si in electrodeposited films increased with increasing melt temperature, reaching approximately 50 nm at 923 K and 20 μm at 1073 K.⁶ Polycrystalline Si solar cells require millimeter-sized grains to

minimize recombination losses at grain boundaries, which can reduce conversion efficiency; however, we have not been able to achieve such sizes in our previous studies.

To address this, we used liquid metal as the electrode for Si deposition. As an initial study, we conducted electrodeposition using a liquid metal electrode held in a small crucible and obtained Si crystals of more than 1 mm, even at 923 K.^{31,32} Solid Si was deposited on the boundary surface between the liquid metal and solid crucible, and not inside the liquid metal electrode. If the liquid metal is maintained in film form on the substrates, a Si film with a large crystal size can be obtained. However, retaining the liquid metal on the substrate in a film form during electrolysis is difficult.

Therefore, we propose a method involving the co-deposition of Si and Zn for Si film deposition, focusing on supplying liquid metal to the substrate via electrolytic reduction rather than using a liquid-metal electrode. A schematic of the proposed electrodeposition method is shown in Fig. 1. The co-deposition of Si and Zn occurs via the simultaneous reduction of Si(IV) and Zn(II) ions in the KF-KCl melt. Consequently, a Si-Zn liquid alloy is formed, and solid Si is deposited from the liquid alloy onto the substrate as electrolysis proceeds. Solid Si with a large grain size, deposited via liquid alloys, eventually forms a film on the substrate. Si films with large grain sizes are obtained by removing the residual Si-Zn liquid alloy from the surface in a post-processing step. When electrodeposition is performed above the melting point of Zn (693 K), a Si-Zn liquid alloy forms, as shown in the Si-Zn binary phase diagram in Fig. 2,³⁶ further supporting the formation of Si-Zn liquid alloys during co-deposition.

In this study, the method involving the co-deposition of Si and Zn was investigated. Initially, cyclic voltammetry was performed to study the behavior of Si(IV) and Zn(II) ions in molten $\text{KF-KCl-K}_2\text{SiF}_6\text{-ZnCl}_2$. Galvanostatic electrolysis was then conducted, and Si deposition on the substrate via liquid Si-Zn alloy was confirmed by analyzing the surface and cross-sectional morphologies. The

[§]ECSJ Student Member

^{§§}ECSJ Active Member

^{§§§}ECSJ Fellow

W. Moteki orcid.org/0000-0003-2657-9519

Y. Norikawa orcid.org/0000-0002-0861-5443

T. Nohira orcid.org/0000-0002-4053-554X

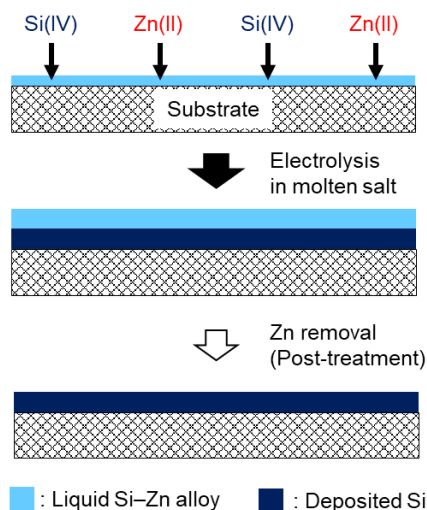


Figure 1. Schematic of the proposed mechanism of Si deposition via co-deposition of Si and Zn.

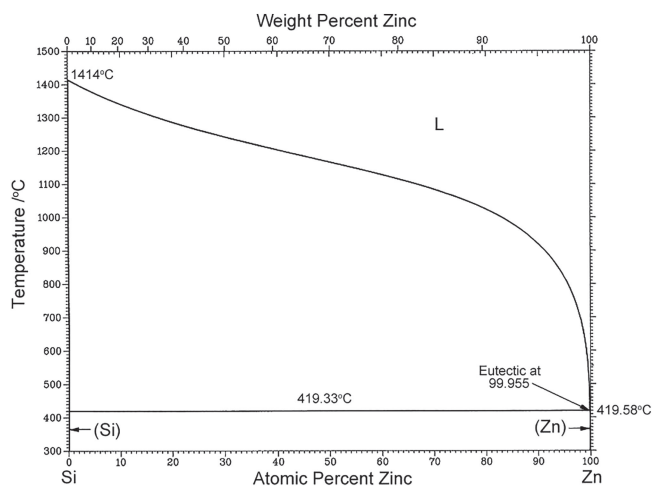


Figure 2. Si–Zn binary phase diagram.³⁶

electrolytic conditions for electrodeposition of highly crystalline Si films were optimized by varying the concentration of ZnCl_2 and current density.

2. Experimental

Figure 3 presents a schematic of the experimental apparatus. Reagent-grade KF (FUJIFILM Wako Pure Chemical Corp., purity > 99.0%) and KCl (FUJIFILM Wako Pure Chemical Corp., purity > 99.5%) were mixed in a eutectic composition (KF : KCl = 45 : 55 mol%, melting point = 873 K, weight = 400 g) and loaded into a graphite crucible (SANKO Co., Ltd., IG-110 grade, o.d. 100 mm \times i.d. 90 mm \times height = 120 mm). The mixture was dried under vacuum at 453 and 773 K for 72 and 24 h, respectively. The dried mixture in the crucible was then placed at the bottom of a stainless-steel vessel in an airtight Kanthal container. Electrochemical measurements were performed at 923 K in a glove box (Yamato, Co., Ltd., pure box system with an electric furnace, ZYS 16–0057) under an Ar atmosphere, maintaining O_2 and H_2O levels below 1 ppm. After blank measurements in KF–KCl, K_2SiF_6 (Junsei Chemical Co., Ltd., purity > 99.0%) was added to the melt to achieve concentrations of 0.1 or 2.0 mol%, and ZnCl_2 (FUJIFILM Wako Pure Chemical Corp., purity > 98.0%) was added to the melt to achieve concentrations of 0.1, 0.5, 1.0, or 2.0 mol%. K_2SiF_6 salt

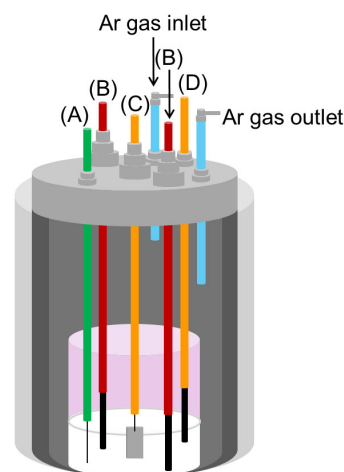


Figure 3. Schematic drawing of the experimental apparatus for the electrochemical measurements: (A) Pt wire electrode (QRE), (B) glassy carbon electrodes (CE), (C) graphite plate electrode (WE), (D) glassy carbon electrode (WE). QRE: quasi reference electrode, CE: counter electrode, WE: working electrode.

was dried in a graphite crucible at 453 K for 10 h, 573 K for 10 h, and 673 K for 10 h before use. Moreover, ZnCl_2 salt was dried in an alumina crucible at 453 K for 72 h and 523 K for 24 h before use.

Electrochemical measurements and galvanostatic electrolysis were performed using a three-electrode system equipped with an electrochemical measurement system (Hokuto Denko Corp., HZ-7000). The working electrodes comprised a glassy carbon (GC) rod (Tokai Carbon Co., Ltd., >99.9998%, diameter = 3.0 mm) and a graphite plate (Toyo Tanso Co., Ltd., IG-15, width: 10.0 mm, thickness: 1.0 mm). GC rods were used as the counter electrodes. A platinum wire (Tanaka Kikinokogyo Co., Ltd., >99.98% purity, diameter = 1.0 mm) was used as the quasi-reference electrode. The potential of the quasi-reference electrode was calibrated considering the dynamic Cl_2/Cl^- potential measured on the GC rod.

Prior to each instrumental analysis, any salt adhering to the surface of samples after electrodeposition was removed by washing with distilled water. The samples were then immersed in distilled water at 303 K for 30 min. Subsequently, the surface was washed with distilled water at 303 K. Finally, ethanol was poured over the samples, which were then dried under cold air.

Surfaces and cross sections of the prepared samples were observed using scanning electron microscopy (SEM; Thermo Fisher Scientific Inc., Phenom Pro Generation 5). The deposits were also characterized using energy-dispersive X-ray spectroscopy (EDX; Thermo Fisher Scientific Inc., SEI200–8001) and X-ray diffraction (XRD; Rigaku Corp., Ultima IV, Cu- $\text{K}\alpha$ line) analysis. For the cross-sectional SEM observation, the samples were embedded in resin (Nisshin ES Co., Ltd., room temperature curing epoxy resin NER-814, medium) and then polished using emery paper (#320, #600), abrasives (SANKEI Co., Ltd., polycrystalline diamond suspension (diameter = 9 and 3 μm), and high-purity alumina (diameter = 0.05 μm)) using a rotary polishing machine (Buehler, Ecomet III). After polishing, the samples were coated with Au using an ion sputtering apparatus (Hitachi, Ltd., E-101) to ensure conductivity. To analyze the surface morphology of Si film, any residual Zn on the deposit was dissolved in 50 mL of HCl solution (20 wt%).

3. Results and Discussions

3.1 Electrochemical behavior of Si(IV) and Zn(II) ions

Cyclic voltammetry was performed to study the reduction behavior of Si(IV) and Zn(II) ions. Figure 4 shows a cyclic

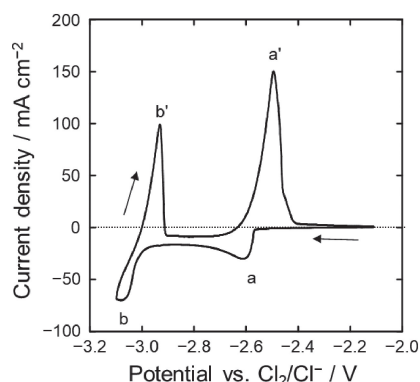
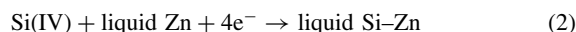


Figure 4. Cyclic voltammogram at a glassy carbon electrode in molten KF–KCl–K₂SiF₆ (0.1 mol%)–ZnCl₂ (0.1 mol%) at 923 K. Scan rate: 0.10 V s⁻¹.

voltammogram of a GC electrode in molten KF–KCl at 923 K with 0.1 mol% K₂SiF₆ and ZnCl₂. IR correction was performed with a feedback rate of 80 %. When the potential was scanned from the rest potential toward the negative side, the cathodic current peaks (a) and (b) were observed around -2.6 V vs. Cl₂/Cl⁻ and -3.1 V, respectively. In our previous study using liquid Zn electrodes, we reported that the rest potential of liquid Zn electrodes was more positive than the Si–Zn liquid alloy formation potential.³¹ Therefore, the cathodic current peak around -2.6 V is attributed to the reduction of Zn(II) ions, as expressed in reaction (1).



The cathodic current peak around -3.1 V is attributed to the Si–Zn liquid alloy formation, as expressed in reaction (2).



As shown in Fig. 2, only 1 at% of Si dissolves in liquid Zn at 923 K.³⁶ Although Si can supersaturate in liquid Zn during the short period of CV measurement, the solid Si formation expressed in reaction (3) is considered to progress simultaneously with the reaction described in reaction (2).



When the potential was reversed and scanned, the oxidation currents (a') and (b') corresponding to (a) and (b), respectively, were observed. These currents result from the reverse reactions, as described in reactions (1)–(3). The above results indicated the reduction of Si(IV) ions during electrolysis at a current exceeding the diffusion-limiting current of the Zn(II) ions, signifying the feasibility of co-deposition of Si and Zn.

3.2 Si deposition via Si–Zn liquid alloy during co-deposition

To confirm Si deposition via Si–Zn liquid alloy during co-deposition, we performed galvanostatic electrolysis on a graphite substrate in molten KF–KCl–K₂SiF₆ (2.0 mol%)–ZnCl₂ (1.0 mol%) at a current density of 150 mA cm⁻² and a charge density of 90 C cm⁻². During electrolysis, the potential was more negative than -3.0 V vs. Cl₂/Cl⁻, indicating the occurrence of co-deposition. As shown in the optical image in Fig. 5a, the obtained sample exhibits a metallic luster across the entire surface, indicating that the Si–Zn alloy formed a film covering the electrode surface. Further detailed observations using SEM (Fig. 5b) and EDX analysis confirmed that the surface is covered with Zn. EDX mapping and spectrum (Fig. S1) showed that the entire surface was covered with Zn and only Zn and Si were detected.

Electrodeposition was performed in molten KF–KCl–ZnCl₂ (1.0 mol%) without Si(IV) ions, using a graphite substrate as the electrode at a current density of 150 mA cm⁻² and a charge density

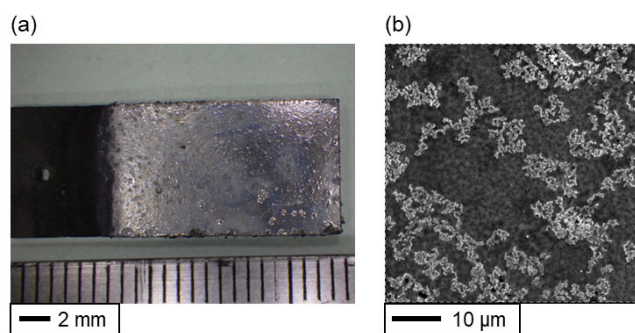


Figure 5. (a) Photograph and (b) surface SEM image of sample obtained by galvanostatic electrolysis of graphite plate electrode at 150 mA cm⁻² for 90 C cm⁻² in molten KF–KCl–K₂SiF₆ (2.0 mol%)–ZnCl₂ (1.0 mol%) at 923 K.

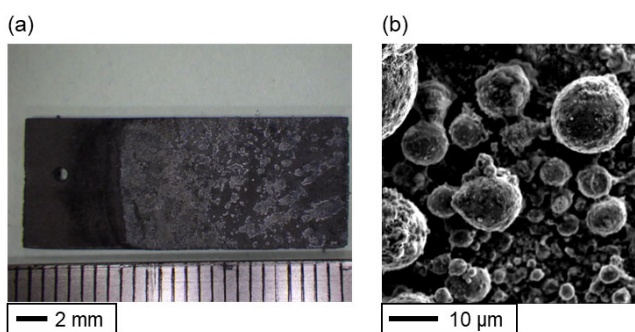


Figure 6. (a) Photograph and (b) surface SEM image of sample obtained by galvanostatic electrolysis of a graphite plate electrode at 150 mA cm⁻² for 90 C cm⁻² in molten KF–KCl–ZnCl₂ (1.0 mol%) at 923 K.

of 90 C cm⁻². The weight change was extremely small, and no metallic luster was observed in the optical image (Fig. 6a). The SEM image shown in Fig. 6b and the EDX analysis results show that Zn was electrodeposited in a spherical morphology on the substrate. These observations confirmed that the reduction of Zn(II) ions alone did not produce a uniform Zn film on the graphite substrate. As liquid Zn did not wet graphite well, only a part of Zn remained on the surface, and the shape was spherical. Unlike the electrodeposits in a bath containing only the Zn(II) ions, the Si–Zn liquid alloy remained nearly entirely on the surface of electrodeposits, attributable to the presence of Si. The good bonding between Si and graphite enabled the Si–Zn liquid alloys to remain on the substrate.

This finding indirectly indicated that Si–Zn was deposited. To verify the above observation, we observed cross-sectional SEM images and performed EDX mapping. Figures 7a and 7b show the cross-sectional SEM images and EDX mapping of the sample, respectively. Two-layered electrodeposits were observed on the substrate in the SEM images. EDX mapping confirmed that the layer closest to the substrate was Si and the layer on the molten salt side was Zn. The Si layer was assumed to be deposited from the Si–Zn liquid alloy during electrolysis, confirming that Si was deposited via the Si–Zn liquid alloy during co-deposition.

To confirm that the deposits were crystalline Si, XRD analysis was conducted. Figure 8 shows the XRD pattern of the sample shown in Fig. 5 after removing Zn via HCl treatment. The diffraction peaks except for those of the graphite substrate were attributed to Si.

3.3 Electrolysis conditions for highly crystalline Si films

To investigate the conditions for obtaining highly crystalline Si

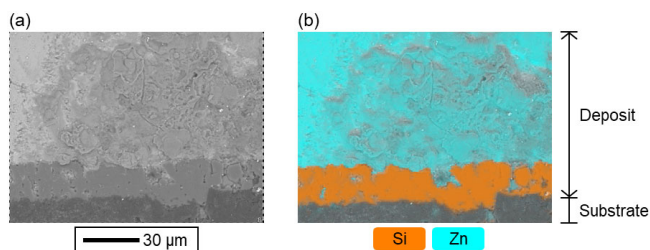


Figure 7. (a) Cross-sectional scanning electron microscopy (SEM) images and (b) energy-dispersive X-ray spectroscopy (EDX) mappings of samples obtained by galvanostatic electrolysis of graphite plate electrode for 90 C cm^{-2} in molten $\text{KF-KCl-K}_2\text{SiF}_6$ (2.0 mol%)- ZnCl_2 (1.0 mol%) at 923 K. Current density was 150 mA cm^{-2} .

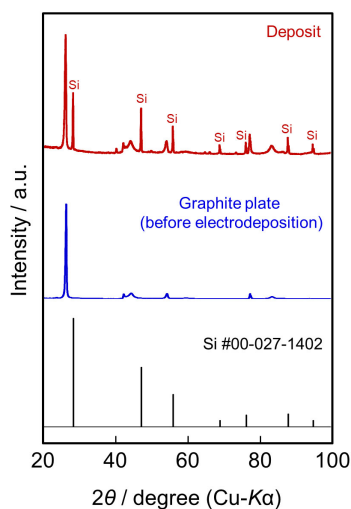


Figure 8. XRD pattern of the sample shown in Fig. 5 after removing Zn via HCl treatment.

films via co-deposition, we performed electrolysis using different ZnCl_2 concentrations and current densities. Initially, electrodeposition was performed on graphite substrates in molten $\text{KF-KCl-K}_2\text{SiF}_6$ (2.0 mol%)- ZnCl_2 (0.5 mol%) at a current density of $100\text{--}200 \text{ mA cm}^{-2}$ and a charge density of 90 C cm^{-2} . Under these conditions, Zn deposit was granular and did not cover the entire surface. Cross-sectional SEM images and EDX mappings of the sample after electrodeposition, particularly where Zn is present on the surface, are shown in Fig. 9. Under the conditions of (a) 100 and (b) 150 mA cm^{-2} , distinct Si and Zn layers were formed with the Si layer closest to the substrate. Despite the incomplete surface coverage by Zn, solid Si was deposited on the graphite substrate from the Si-Zn liquid alloy. Conversely, at a current density of (c) 200 mA cm^{-2} , the deposit on the substrate was not divided into two layers of Si and Zn. The finding could be attributed to the large reduction in the amount of Si(IV) ion compared to that of the Zn(II) ion reduction, resulting in rapid deposition of solid Si from the liquid alloy. Furthermore, deposition occurred on top of the protruding deposits, resulting in a dendrite-like shape.

Next, electrodeposition was carried out on graphite substrates in molten $\text{KF-KCl-K}_2\text{SiF}_6$ (2.0 mol%)- ZnCl_2 (1.0 mol%) at a current density of $100\text{--}200 \text{ mA cm}^{-2}$ and a charge density of 90 C cm^{-2} . At this ZnCl_2 concentration, Zn uniformly covered the entire surface of the deposit. Cross-sectional SEM images and EDX mappings of the samples after electrodeposition are shown in Fig. 10. At current densities of (a) 100 and (b) 150 mA cm^{-2} , the Si and Zn layers on

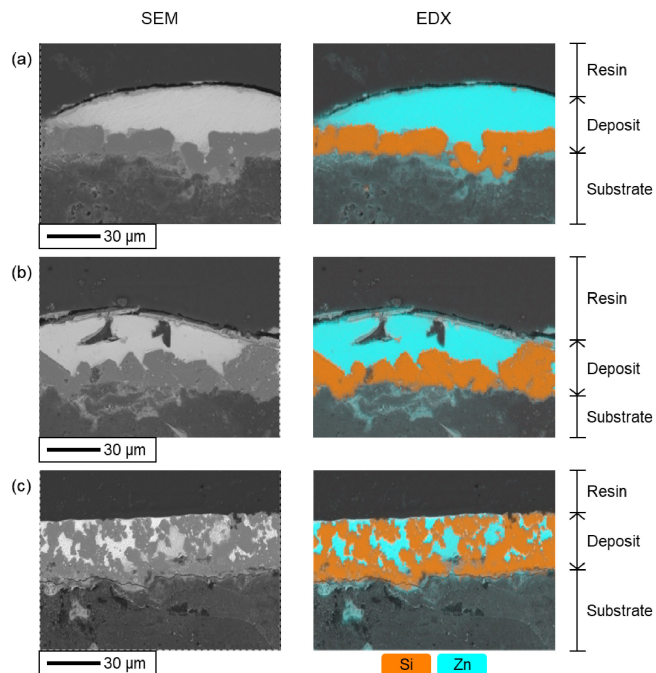


Figure 9. Cross-sectional SEM images and EDX mappings of the samples obtained by galvanostatic electrolysis of graphite plate electrode for 90 C cm^{-2} in molten $\text{KF-KCl-K}_2\text{SiF}_6$ (2.0 mol%)- ZnCl_2 (0.5 mol%) at 923 K. Current densities were (a) 100 mA cm^{-2} , (b) 150 mA cm^{-2} , and (c) 200 mA cm^{-2} .

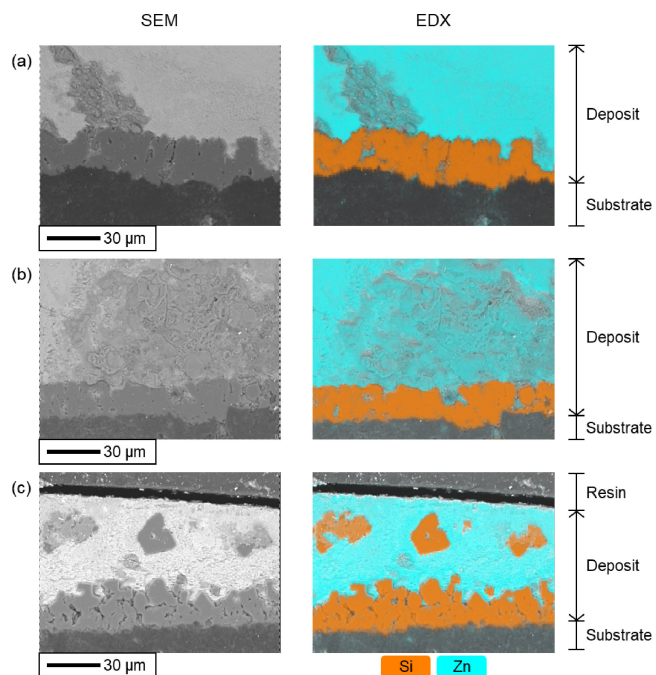


Figure 10. Cross-sectional SEM images and EDX mappings of the samples obtained by galvanostatic electrolysis of graphite plate electrode for 90 C cm^{-2} in molten $\text{KF-KCl-K}_2\text{SiF}_6$ (2.0 mol%)- ZnCl_2 (1.0 mol%) at 923 K. Current densities were (a) 100 mA cm^{-2} , (b) 150 mA cm^{-2} , and (c) 200 mA cm^{-2} .

the graphite substrate were observed in sequence from the substrate. At a current density of (c) 200 mA cm^{-2} , a Si layer was deposited on the substrate; however, Si lumps were found in the Zn layer above it, likely representing cross-sectional observations of dendrite-like Si deposits. These results suggest that the appropriate current density

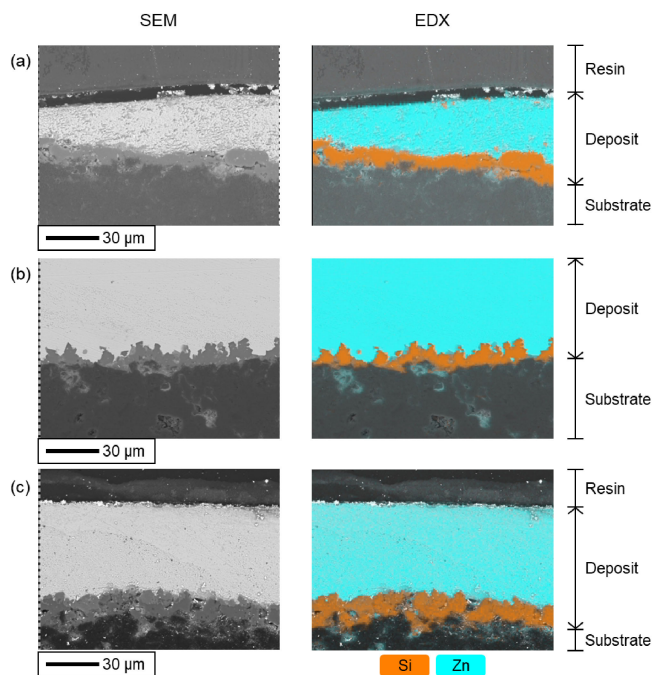


Figure 11. Cross-sectional SEM images and EDX mappings of the samples obtained by galvanostatic electrolysis of a graphite plate electrode for 90 C cm^{-2} in molten $\text{KF-KCl-K}_2\text{SiF}_6$ (2.0 mol%)- ZnCl_2 (2.0 mol%) at 923 K. Current densities were (a) 200 mA cm^{-2} , (b) 250 mA cm^{-2} , and (c) 300 mA cm^{-2} .

for electrolysis at a ZnCl_2 concentration of 1.0 mol% was (a) 100 or (b) 150 mA cm^{-2} .

Furthermore, electrodeposition was carried out on graphite substrates in molten $\text{KF-KCl-K}_2\text{SiF}_6$ (2.0 mol%)- ZnCl_2 (2.0 mol%) at current densities in the range $200\text{--}300\text{ mA cm}^{-2}$ and a charge density of 90 C cm^{-2} . At this ZnCl_2 concentration, the entire surface of the deposit was covered with Zn. Cross-sectional SEM images and EDX mappings of the samples after electrodeposition are shown in Fig. 11. At all values of current densities, the amount of Si relative to the overall thickness of the deposit was less than that for a ZnCl_2 concentration of 1.0 mol%. This result was attributed to the larger amount of reduced Zn, and smaller amount of reduced Si compared to those obtained in the melt with 1.0 mol% of ZnCl_2 .

A comparison of the cross-sectional morphology of the electrodeposits obtained in the above three melts enabled us to construe a relationship between the ZnCl_2 concentration and the morphology of electrodeposits. In the melt containing 0.5 mol% ZnCl_2 , Zn did not cover the entire surface of the electrode owing to the low concentration of Zn(II) ions present in the melt. Consequently, only a small amount of Zn was reduced compared to that required to cover the entire electrode surface. In the melt containing 2.0 mol% ZnCl_2 , Zn covered the entire electrode surface. However, the amount of reduced Si was small, raising concerns regarding the decrease in the current efficiency of the target product of the Si film. The melt containing 1.0 mol% ZnCl_2 offered better conditions than the melt containing 0.5 mol% ZnCl_2 because Zn covered the entire substrate surface of the deposit. Furthermore, considering the current efficiency for the target Si film, this melt is superior to the melt containing 2.0 mol% ZnCl_2 . Based on the cross-sectional morphology results described above, electrolysis at a current density of 100 or 150 mA cm^{-2} in a melt with a ZnCl_2 concentration of 1.0 mol% was considered to be an optimal condition.

The morphology of the electrodeposited Si was observed after removing Zn via HCl treatment. The SEM images of the electrode surfaces after electrolysis and HCl treatment under the respective

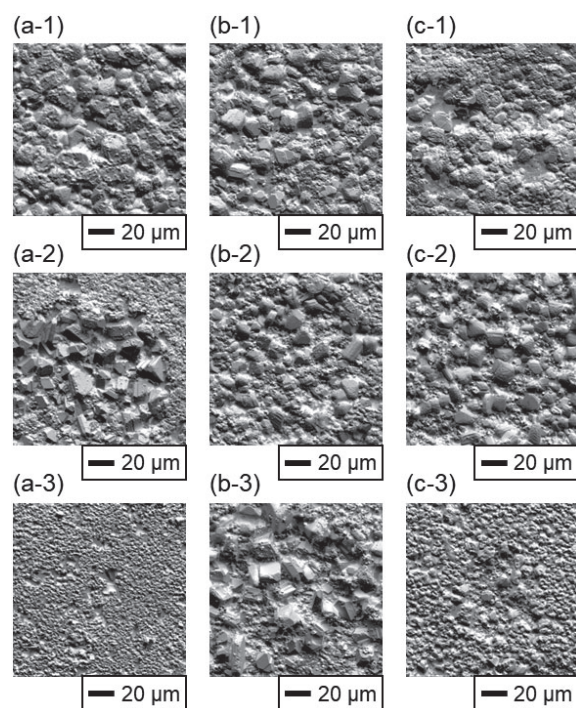


Figure 12. Surface SEM images of samples obtained by galvanostatic electrolysis of a graphite plate electrode for 90 C cm^{-2} in molten $\text{KF-KCl-K}_2\text{SiF}_6$ - ZnCl_2 at 923 K. K_2SiF_6 concentration was 2.0 mol%. ZnCl_2 concentrations were (a) 0.5, (b) 1.0, and (c) 2.0 mol%. (a) Current densities were (a-1) 100 mA cm^{-2} , (a-2) 150 mA cm^{-2} , and (a-3) 200 mA cm^{-2} . (b) Current densities were (b-1) 100 mA cm^{-2} , (b-2) 150 mA cm^{-2} , and (b-3) 200 mA cm^{-2} . (c) Current densities were (c-1) 200 mA cm^{-2} , (c-2) 250 mA cm^{-2} , and (c-3) 300 mA cm^{-2} .

electrolysis conditions are shown in Fig. 12. In Figs. 12a-3, 12c-1, and 12c-3, the crystal size of the electrodeposited Si is small, so the electrolysis conditions are unfavorable. In the samples obtained under electrolytic conditions excluding these three, crystals with a size of $20\text{ }\mu\text{m}$ or more were observed. These values were clearly larger than the 50 nm crystal size that was obtained in our previous study on Si electrodeposition at a solid Ag electrode in $\text{KF-KCl-K}_2\text{SiF}_6$ at 923 K.⁶ The surface morphology demonstrated the effect of Si deposition via the Si-Zn liquid alloy on the grain size of the Si crystals in the film, as expected from our previous report.³¹ The electrodeposits obtained under the aforementioned conditions, shown in Figs. 12b-1 and 12b-2, which yield a good cross-sectional morphology, exhibit a good surface morphology because of their large grain sizes. Based on the aforementioned results, the optimal current density conditions for achieving the desired results were considered to be approximately in the range $100\text{--}150\text{ mA cm}^{-2}$.

4. Conclusions

The co-deposition of Si and Zn resulted in the formation of highly crystalline Si films on graphite substrates in molten KF-KCl at 923 K. Cyclic voltammetry revealed the reduction of Si(IV) and Zn(II) ions, with Si deposited via a Si-Zn liquid alloy during co-deposition. In the electrodeposits obtained by co-deposition, a Si layer was observed on the graphite substrate with a Zn layer on top. By varying the concentration of ZnCl_2 and current density, optimal conditions for obtaining superior Si films were identified. The Si films obtained through co-deposition exhibited larger crystal sizes than those obtained via electrodeposition without ZnCl_2 , confirming deposition via Si-Zn liquid alloying.

Acknowledgments

This study was supported by Grant-in-Aid for Scientific Research A (Grant Number 21H04620) from the Japan Society for the Promotion of Science (JSPS). This study was partially supported by JSPS Fellows (Grant Number 24KJ1394).

CRedit Authorship Contribution Statement

Wataru Moteki: Data curation (Lead), Funding acquisition (Equal), Investigation (Lead), Methodology (Equal), Validation (Equal), Writing – original draft (Lead)
 Yutaro Norikawa: Conceptualization (Equal), Data curation (Equal), Methodology (Lead), Supervision (Equal), Validation (Equal), Writing – review & editing (Equal)
 Toshiyuki Nohira: Conceptualization (Equal), Funding acquisition (Equal), Methodology (Equal), Supervision (Equal), Validation (Equal), Writing – review & editing (Equal)

Data Availability Statement

The data that support the findings of this study are openly available under the terms of the designated Creative Commons License in J-STAGE Data listed in D1 of References.

Conflict of Interest

There are no conflicts of interest to declare.

Funding

Japan Society for the Promotion of Science: 21H04620
 Japan Society for the Promotion of Science: 24KJ1394

References

- D1. W. Moteki, Y. Norikawa, and T. Nohira, *J-STAGE Data*, <https://doi.org/10.50892/data.electrochemistry.28013060>, (2024).
- International Energy Agency, *Trends in Photovoltaic Applications 2023*, IEA PVPS (2023).
 - K. Yasuda and T. Nohira, *High. Temp. Mater. Proc.*, **41**, 247 (2022).
 - K. Maeda, K. Yasuda, T. Nohira, R. Hagiwara, and T. Homma, *J. Electrochem. Soc.*, **162**, D444 (2015).
 - K. Yasuda, K. Maeda, T. Nohira, R. Hagiwara, and T. Homma, *J. Electrochem. Soc.*, **163**, D95 (2016).
 - K. Yasuda, K. Maeda, R. Hagiwara, T. Homma, and T. Nohira, *J. Electrochem. Soc.*, **164**, D67 (2017).
 - K. Yasuda, K. Saeki, T. Kato, R. Hagiwara, and T. Nohira, *J. Electrochem. Soc.*, **165**, D825 (2018).
 - K. Yasuda, T. Kato, Y. Norikawa, and T. Nohira, *J. Electrochem. Soc.*, **168**, 112502 (2021).
 - Y. Norikawa, A. Kondo, K. Yasuda, and T. Nohira, *Electrochim. Acta*, **434**, 141255 (2022).
 - U. Cohen and R. A. Huggins, *J. Electrochem. Soc.*, **123**, 381 (1976).
 - G. M. Rao, D. Elwell, and R. S. Feigelson, *J. Electrochem. Soc.*, **127**, 1940 (1980).
 - A. Elwell and R. Wise, *J. Antimicrob. Chemother.*, **10**, 560 (1982).
 - K. S. Osen, A. M. Martinez, S. Rolseth, H. Gudbrandsen, M. Juel, and G. M. Haarberg, *ECS Trans.*, **33**, 429 (2010).
 - A. L. Bieber, L. Massot, M. Gibilaro, L. Cassayre, P. Taxi, and P. Chamelot, *Electrochim. Acta*, **62**, 282 (2012).
 - G. M. Haarberg, L. Famiyeh, A. M. Martinez, and K. S. Osen, *Electrochim. Acta*, **100**, 226 (2013).
 - Y. J. Hu, X. Wang, J. S. Xiao, J. G. Hou, S. Q. Jiao, and H. M. Zhu, *J. Electrochem. Soc.*, **160**, D81 (2013).
 - Y. Sakanaka and T. Goto, *Electrochim. Acta*, **164**, 139 (2015).
 - Y. Suzuki, Y. Inoue, M. Yokota, and T. Goto, *J. Electrochem. Soc.*, **166**, D564 (2019).
 - R. Boen and J. Bouteillon, *J. Appl. Electrochem.*, **13**, 277 (1983).
 - T. Matsuda, S. Nakamura, K. Ide, K. Nyudo, S. Yae, and Y. Nakato, *Chem. Lett.*, **25**, 569 (1996).
 - S. V. Devyatkin, *J. Min. Metall. Sect. B*, **39**, 303 (2003).
 - J. Zhao, H. Y. Yin, T. H. Lim, H. W. Xie, H. Y. Hsu, F. Forouzan, and A. J. Bard, *J. Electrochem. Soc.*, **163**, D506 (2016).
 - Y. Sakanaka, A. Murata, T. Goto, and K. Hachiya, *J. Alloys Compd.*, **695**, 2131 (2017).
 - X. Zou, L. Ji, X. Yang, T. Lim, E. T. Yu, and A. J. Bard, *J. Am. Chem. Soc.*, **139**, 16060 (2017).
 - Y. Zhang, Y. Zhang, X. Li, J. Liu, M. Zhang, X. Yang, M. Huang, M. Xu, P. Dong, and Z. Zhou, *JOM*, **72**, 2245 (2020).
 - A. A. Andriiko, E. V. Panov, O. I. Boiko, B. V. Yakovlev, and O. Y. Borovik, *Russ. J. Electrochem.*, **33**, 1343 (1997).
 - S. V. Kuznetsova, V. S. Dolmatov, and S. A. Kuznetsov, *Russ. J. Electrochem.*, **45**, 742 (2009).
 - Y. P. Zaykov, S. I. Zhuk, A. V. Isakov, O. V. Grishenkova, and V. A. Isaev, *J. Solid State Electrochem.*, **19**, 1341 (2015).
 - J. Peng, H. Yin, J. Zhao, X. Yang, A. J. Bard, and D. R. Sadoway, *Adv. Funct. Mater.*, **28**, 1703551 (2018).
 - S. I. Zhuk, V. A. Isaev, O. V. Grishenkova, A. V. Isakov, A. P. Apisarov, and Y. P. Zaykov, *J. Serb. Chem. Soc.*, **82**, 51 (2017).
 - S. I. Zhuk, A. V. Isakov, A. P. Apisarov, O. V. Grishenkova, V. A. Isaev, E. G. Vovkotrub, and Y. P. Zaykov, *J. Electrochem. Soc.*, **164**, H5135 (2017).
 - W. Moteki, Y. Norikawa, and T. Nohira, *J. Electrochem. Soc.*, **170**, 062506 (2023).
 - W. Moteki, Y. Norikawa, and T. Nohira, *J. Electrochem. Soc.*, **171**, 082501 (2024).
 - G. M. Haarberg, T. Kato, Y. Norikawa, and T. Nohira, *ECS Trans.*, **89**, 29 (2019).
 - J. R. Rumble, *CRC Handbook of Chemistry and Physics* (99th ed.), CRC Press, Boca Raton (2018).
 - Y. Norikawa and T. Nohira, *Acc. Chem. Res.*, **56**, 1698 (2023).
 - T. B. Massalski, H. Okamoto, P. R. Subramanian, and L. Kacprzak, *Binary Alloy Phase Diagrams* (2nd ed.), ASM International, Materials Park, Ohio (1990), CD-ROM version 1.0.